Hindawi
Bioinorganic Chemistry and Applications
Volume 2017, Article ID 6398167, 16 pages
https://doi.org/10.1155/2017/6398167

Research Article

Bioactive Potential of 3D-Printed Oleo-Gum-Resin Disks: *B. papyrifera*, *C. myrrha*, and *S. benzoin* Loading Nanooxides—TiO_2, P25, Cu_2O, and MoO_3

Diogo José Horst,[1] Sergio Mazurek Tebcherani,[2] Evaldo Toniolo Kubaski,[3] and Rogério de Almeida Vieira[4]

[1]*Federal University of Technology-Paraná, 84016-210 Ponta Grossa, PR, Brazil*
[2]*Department of Production Engineering, Federal University of Technology-Paraná, 84016-210 Ponta Grossa, PR, Brazil*
[3]*Department of Materials Science, State University of Ponta Grossa, 84030-900 Ponta Grossa, PR, Brazil*
[4]*Department of Earth and Exact Sciences, Federal University of São Paulo, 89972-270 São Paulo, SP, Brazil*

Correspondence should be addressed to Diogo José Horst; diogohorst@gmail.com

Received 1 March 2017; Accepted 20 April 2017; Published 25 July 2017

Academic Editor: Francesco P. Fanizzi

This experimental study investigates the bioactive potential of filaments produced via hot melt extrusion (HME) and intended for fused deposition modeling (FDM) 3D printing purposes. The oleo-gum-resins from benzoin, myrrha, and olibanum in pure state and also charged with 10% of metal oxide nanoparticles, TiO_2, P25, Cu_2O, and MoO_3, were characterized by ultraviolet-visible (UV-Vis) and Fourier transform infrared (FTIR) spectroscopy, energy-dispersive X-ray microanalysis (EDXMA), scanning electron microscopy (SEM), and differential scanning calorimetry (DSC). Disks were 3D-printed into model geometries (10 × 5 mm) and the disk-diffusion methodology was used for the evaluation of antimicrobial and antifungal activity of materials in study against the clinical isolates: *Staphylococcus aureus, Pseudomonas aeruginosa, Escherichia coli*, and *Candida albicans*. Due to their intrinsic properties, disks containing resins in pure state mostly prevent surface-associated growth; meanwhile, disks loaded with 10% oxides prevent planktonic growth of microorganisms in the susceptibility assay. The microscopy analysis showed that part of nanoparticles was encapsulated by the biopolymeric matrix of resins, in most cases remaining disorderly dispersed over the surface of resins. Thermal analysis shows that plant resins have peculiar characteristics, with a thermal behavior similar to commercial available semicrystalline polymers, although their structure consists of a mix of organic compounds.

1. Introduction

Infections caused by pathogenic microorganisms are of great concern in many fields [1]. Hospital-acquired infections are one of the major problems increasing mortality and morbidity. Microbial contamination may occur from various sources and invasive interventions [2]. *Staphylococcus aureus* is a Gram-positive major human pathogen that causes skin and soft-tissue infections, life-threatening infections such as pneumonia and sepsis, and toxinoses including toxic shock syndrome [3]. *Pseudomonas aeruginosa* is a Gram-negative bacillus that is rapidly becoming one of the major causes of opportunistic and nosocomial infections which have become a worldwide problem [4]. *Escherichia coli* is a Gram-negative pathogen which has been regarded as an important indicator bacterium; it causes severe diseases, such as hemolytic uremic syndrome (HUS), hemorrhagic colitis [5], and thrombotic thrombocytopenic purpura which can be fatal in some cases [6, 7]. *Candida albicans* is renowned as the leading fungal pathogen of oral candidosis, which manifests in a variety of clinical guises ranging from common denture associated infections in otherwise healthy individuals to systemic infections in human immunodeficiency virus disease [8, 9].

Although bacteria have shown the ability to acquire resistance to many antibiotics, however, in nature, there are several examples of antibiotics to which resistance

has not yet developed [10, 11]. The history of medicine and pharmacy is well known for using plant oleo-gum-resins and extracts in curing diseases; these are known to have analgesic, antioxidant, antifungal, antiseptic, antibacterial, astringent, sedative, and stimulant therapeutic properties, among others [12–21]. The bioactivity of oils and extracts obtained species *Commiphora myrrha, Styrax benzoin*, and *Boswellia papyrifera* has been investigated by several researches [22–31]; these aromatic resins basically consist of monoterpenes (C10H16), triterpenes (C30H48), and sesquiterpenes (C15H24) with unique combinations, besides benzoic, myrrholic, and boswellic acids, respectively [32–37]; the demonstration of the presence of secondary metabolites in medicinal plants oils, extracts, and resins provides a scientific validation for the popular use of these plants [38–42].

Besides that, a greener approach for the biosynthesis of colloidal metal nanoparticles and dispersion/encapsulation of drugs using natural oleo-gum-resins has been suggested as being effective and more environmental friendly [43–49]. Moreover, the development of multifunctional nanocomposite materials with enhanced mechanical and antimicrobial properties has been studied [50–52]. Indeed, nanoparticles (NPs) are widely used in the field of healthcare, presenting numerous advantages in medical and biotechnological applications [53, 54] and increasingly attracting researchers due to their unique properties, such as submicrometer size (1–100 nm), large surface-to-volume ratio, and advanced reactivity [55, 56].

It is imperative to improve the applicability of 3D printing for pharmaceutical purposes by searching novel materials. The investigation of different physicochemical properties and adequate processing parameters of such materials is important for successful additive manufacturing of personalized geometries [57]. In the last years, the use of 3D printing for the development of drug delivery systems, medical devices, bone tissue engineering, and antimicrobial materials has shown promising results with a large possibility of applications [58–61]. Beyond that, the use of hot melt extrusion (HME) in the fabrication of novel antimicrobial filaments for pharmaceutical application has steadily increased [62–67]. Nature can combine brittle minerals and organic molecules into hybrid composites that are highly organized to achieve exceptional properties [68, 69]; organic-inorganic hybrid nanostructures and materials on their basis are promising class of multifunctional advanced materials [70, 71]. Within this context, the purpose of this study was to evaluate the potential of hybrid engineered materials intended for fused deposition modeling (FDM) 3D printing, testing its bioactivity against clinical pathogenic organisms including Gram-positive, Gram-negative bacteria, and fungus.

2. Materials and Methods

2.1. Materials and Reagents. Oleo-gum-resins from benzoin *(Styrax benzoin)* harvested in Singapore, olibanum *(Boswellia papyrifera)* originally from Ethiopia, and myrrh *(Commiphora myrrha)* from Somalia were purchased from Mountain Rose Herbs (Eugene, Oregon, USA). Titanium dioxide (TiO_2), anatase (P25), molybdenum trioxide (MoO_3), and copper I (Cu_2O) oxide were purchased from Plasmachem (GmbH, Germany); the nanoparticles have sizes between 10 nm to 1 nm. Prior to testing, all materials were sterilized using UV radiations. Clinical isolates of *Staphylococcus aureus* ATCC 6538*; Pseudomonas aeruginosa* ATCC 9027; *Escherichia coli* ATCC 8739; and *Candida albicans* ATCC 2091 were purchased from the American Type Culture Collection (ATCC, Manassas, VA, USA). Mueller-Hinton agar and Sabouraud dextrose agar were purchased from Kasvi (Curitiba, PR, Brazil).

2.2. Preparation of Materials. Resins in powder form in pure state and also loaded with 10% (w.t) oxides were added to a hot melt desktop screw extruder (Filastruder, GA, USA) forming printable filaments measuring 1.75 mm diameter; the extrusion was performed at temperatures within 70–85°C and the materials were cooled at ambient conditions; the extrusion speed was maintained at 20 rpm. In sequence, disks (10 × 5 mm) were manufactured using a FDM 3D printer (Prusa Mendel–I3, USA). The printing temperature was maintained at 80°C and the heating of table was maintained at 60°C; the printing feeding speed was maintained at 10 mm/min; the output measure of the hot end is 0.4 mm.

2.3. Susceptibility Assay In Vitro. Mueller-Hinton agar (MHA) was used to determine the antimicrobial activity of materials in study against bacteria and Sabouraud dextrose agar (SDA) was prepared for fungi; the agar media were prepared by following manufacturer instructions. The plates were autoclaved, in sequence; holes were made for insertion of sampling disks. Using a sterile transfer loop, suspensions containing 5×10^6 CFU/mL^{-1} were inoculated in the agar media. Then, the plates were incubated at bacteriological greenhouse during 48 hours at 34°C, with growth checks performed at every 6 hours. The bioactivity of materials was evaluated by comparing the inhibition zone (diameter in mm) and also number of colony forming units (CFU) in relation to the control plates with positive growth. The semiquantitative K-B disk-diffusion method was used to determine the antimicrobial and antifungal activity of materials [72, 73]. To obtain a more accurate counting of the viable cells, the software ImageJ with the plugin automated colony counting was used [74–76].

2.4. Scanning Electron Microscopy (SEM) and Energy-Dispersive X-Ray Microanalysis (EDXMA). Scanning electron microscopy (SEM) analysis was performed using equipment Jeol (JSM-6610LV). Samples of resins in pure state and resins loading metal oxides were placed on a carbon tape and subjected to a vacuum and electron beam. The structural identification of the samples was performed by X-rays diffraction measurements; the equipment used was a Bruker diffractometer (D8 Advance) equipped with a lynx-eye detector. We used a copper X-ray generator tube with radiation Kalfa 1 = 1.5406 A. The power was adjusted to 1600 W (40 kV and 40 mA) for evaluating the signals diffracted in the region between 20° and 120° 2 theta in step 0.025°/s. Samples were prepared in order to avoid any

preferential orientation of hkl planes in a standard circular sample holder with a diameter of approximately 2.5 cm.

2.5. UV-Visible (UV-Vis) Absorption and Fourier Transform Infrared (FTIR) Spectroscopy. Spectroscopy analysis in the ultraviolet-visible region (UV-Vis) was carried out utilizing Shimadzu equipment (UV-1800) calibrated at a bandwidth of 1 nm; the wavelength range was maintained from 300 to 900 nm. The Fourier transformed infrared (FTIR) spectroscopy measurements were performed using a Shimadzu Spectrometer Prestige 21 (Shimadzu Corporation, Koyoto, Japan) with a resolution of 2 cm^{-1}. The measurements were carried out on KBr pellets which have transparency in the infrared region 400–4000 cm^{-1}. In this context, the powder samples resins and resins oxides (1 mg) were ground with KBr (300 mg, spectroscopic, high purity). To form the tablets, the mixture was placed in a hydraulic press applying approximately 10 tones, while the air was extracted by a mechanical pump. The FTIR spectra of the samples were recorded at ambient temperature and spectral band between 4000 and 300 cm^{-1}.

2.6. Differential Scanning Calorimetry (DSC). In the calorimetric analysis, samples were weighed (3.0 ± 0.5 mg) and hermetically sealed in aluminum crucibles being placed in a Shimadzu calorimeter model DSC-60 under an atmosphere of nitrogen, flow 50 ml min^{-1}; the heating ratio was maintained from 20°C min^{-1} to 550°C. The heating rate was maintained at 10°/min and the nitrogen flow was 100 ml/min. The equipment was calibrated for temperature with indium standard (156.6 ± 0.3°C) through their melting peak. The enthalpy and heat flow were calibrated using the heat of fusion of indium (28.59 J/g ± 0.30) using the same conditions as the samples. The correction factor was calculated in accordance with the procedures and specifications from Shimadzu.

2.7. Statistical Analysis. For data treatment of the susceptibility assay in vitro, the Experimental Design in Contextualized Blocks was used [77, 78]. In this research, the blocks are the 16 samples (raw data) and the treatments are 15 types of material + control plates, therefore totalizing 16 essays; the assay was carried out in quadruplicate for tested microorganisms; for data treatment, the statistical software SASM-Agri-8.1 was used [79].

2.8. List of Abbreviations. In text, the resins in pure state were identified as follows: *Styrax benzoin* (B pure), *Commiphora myrrha* (M pure), and *Boswellia papyrifera* (P pure). The oxides were identified as titanium dioxide (TiO_2); anatase oxide (P25); copper I (Cu_2O); and molybdenum trioxide (MoO_3), respectively.

3. Results and Discussion

3.1. Susceptibility Assay In Vitro. According to Figure 1(a) during the initial period of 6 hours, the growth of *C. albicans* was inhibited by materials B (pure), B + TiO_2, B + MoO_3, B + Cu_2O, B + P25, P + MoO_3, P + Cu_2O, P + P25, M + MoO_3, M + Cu_2O, B + MoO_3, B + Cu_2O, B + P25, P + Cu_2O, and M + Cu_2O ($p = 0.05$).

In 12-hour testing period, its growth of was limited by resin B (pure), B + TiO_2, B + MoO_3, B + Cu_2O, B + P25, P + TiO_2, P + MoO_3, P + P25, M pure, M + TiO_2, M + P25, B + P25, P + P25, and M + TiO_2. During 24-hour period, its growth was hampered by all materials, with one exception M + MoO_3; at this period, the most efficient materials were B + Cu_2O, B + P25, and P + Cu_2O. At 36 hours, B + Cu_2O, P + Cu_2O, M + Ti_2O, and M + Cu_2O were the most efficient materials. In the test period of 48 hours, its growth was restrained by all materials with one exception in P + P25 and the most efficient materials were B (pure), B + TiO_2, B + MoO_3, B + Cu_2O, P + MoO_3, P + Cu_2O, M (pure), M + TiO_2, and M + MoO3. In short, all materials tested (numerically) impede the proliferation of *C. albicans* ($p = 5\%$), highlighting B + TiO_2, B + MoO_3, B + Cu_2O, P + MoO_3, P + Cu_2O, M (pure), and M + MoO_3 which were the most efficient bioactive materials during the 48-hour assay.

According to Figure 1(b), during initial 6-hour testing period, the most effective materials were B + Cu_2O, P + TiO_2, M (pure), M + Cu_2O, and M + P25. Already during 12-hour testing period, the materials B (pure), B + MoO_3, P + MoO_3, and M + MoO_3 were the most effective. During 24-hour assay, the materials B + TiO_2, B + MoO_3, B + Cu_2O, P + TiO_2, P + Cu_2O, M + TiO_2, M + Cu_2O, and M + P25 were the most efficient and, during 36-hour period, the materials B + MoO_3, P + TiO_2, P + Cu_2O, M + TiO_2, and M + Cu_2O were the most effective. At the final period of 48-hour assay, all materials showed significant effectiveness in relation to the control plate, with only one exception P + P25 ($p = 5\%$). In sum, all materials under study (numerically) prevent the proliferation of *E. coli*, highlighting B + MoO_3, P + Cu_2O, P + TiO_2, and M + TiO_2, which stood out as the most bioactive materials.

In relation to Figure 1(c), during the initial period of 6 hours, among the materials that inhibited the growth of this bacterium, B + MoO_3, B + Cu_2O, P + Cu_2O, and M + P25 stood out. However, in the period of 12 hours, all materials tested showed no significant difference concerning the control plates, being considered ineffective during this period of assay. In 24-hour period, the materials B + Cu_2O, B + TiO_2, B + MoO_3, B + Cu_2O, B + P25, P + MoO_3, M + TiO_2, M + MoO_3, and M + Cu_2O were the most effective in detaining its growth. In the period of 36 hours, B + MoO_3, B + Cu_2O, P + Cu_2O, M + TiO_2, and M + Cu_2O were the most efficient. At the final period of 48 hours, the materials B + MoO_3, B + P25, P + MoO_3, M + TiO_2, and M + MoO_3 were the most effective in inhibiting its growth ($p = 5\%$). In short, all materials (numerically) were effective against the bacteria in question, highlighting B + MoO_3, P + MoO_3, and M + TiO_2 and presenting the higher inhibition rates.

According to Figure 1(d) during the initial period of 6 hours, in all cases, there was no significant difference between the materials and the control plate. However, during 12-hour period, significant differences were noted, highlighting B + MoO_3 and M + MoO_3 which were the most effective in restraining its growth. In the period of 24 hours, in most cases, there was no significant difference between the

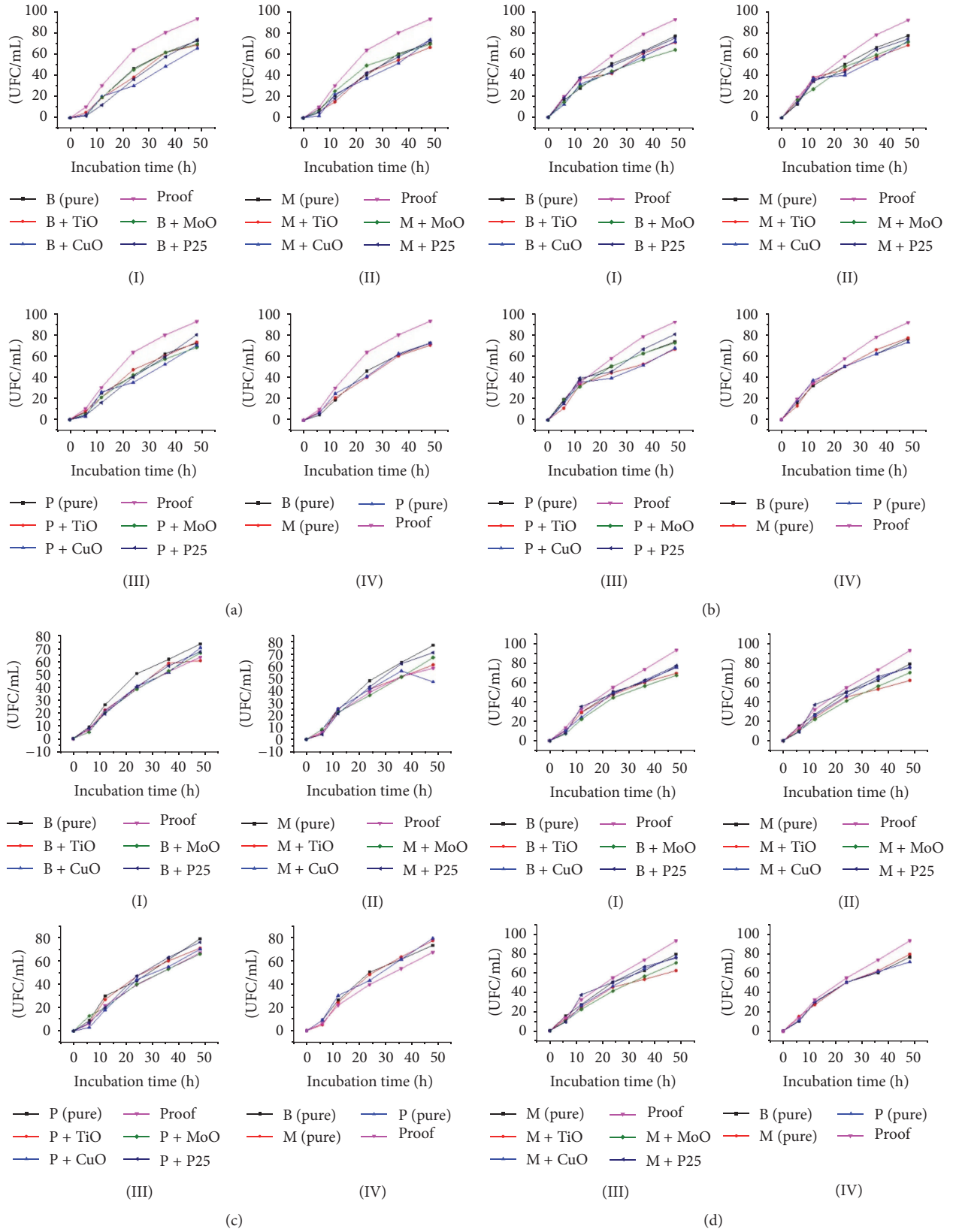

Figure 1: Antibiogram of clinical isolates: (a) refers to *C. albicans*; (b) refers to *E. coli*; (c) refers to *S. aureus*; and (d) refers to *P. aeruginosa* microorganisms.

Table 1: Antibacterial activity of materials against selected pathogenic strains.

Oleo-gum-resin	Inhibition zone (mm)			
Nanooxide	*S. aureus*	*E. coli*	*P. aeruginosa*	*C. albicans*
M (pure)	1.5 ± 1.5	3.0 ± 0.4	5.5 ± 0.6	2.4 ± 3.2
P (pure)	2.0 ± 1.0	3.1 ± 0.5	4.7 ± 0.88	4.4 ± 2.4
B (pure)	1.1 ± 1.1	4.0 ± 0.4	4.0 ± 2.5	1.8 ± 1.8
M + TiO_2	5.2 ± 0.18	8.8 ± 0.32	7.2 ± 0.28	6.8 ± 0.15
M + P25	6.0 ± 0.97	6.4 ± 0.11	6.1 ± 0.35	6.1 ± 0.26
M + MoO_3	5.5 ± 0.22	7.0 ± 0.20	6.6 ± 0.32	6.7 ± 0.92
M + Cu_2O	5.0 ± 0.28	6.5 ± 0.91	6.4 ± 1.57	5.5 ± 0.36
P + TiO_2	5.5 ± 1.55	8.0 ± 0.14	7.7 ± 1.90	6.0 ± 0.21
P + P25	5.8 ± 0.10	5.2 ± 0.26	6.2 ± 0.88	6.0 ± 1.74
P + MoO_3	5.5 ± 0.23	6.5 ± 0.36	7.0 ± 0.30	6.9 ± 1.59
P + Cu_2O	5.6 ± 1.81	8.0 ± 0.53	7.4 ± 1.39	6.6 ± 2.13
B + TiO_2	6.0 + 0.38	7.7 ± 0.77	5.0 ± 1.80	6.8 ± 1.27
B + P25	7.6 ± 0.53	6.2 ± 0.65	4.5 ± 0.36	6.1 ± 2.05
B + MoO_3	6.1 ± 1.70	8.3 ± 0.40	5.2 ± 1.24	6.5 ± 2.46
B + Cu_2O	7.5 ± 1.15	7.0 ± 0.88	4.8 ± 0.36	7.1 ± 2.15

Note. The experiments were done in quadruplicate and the results were interpreted in terms of standard deviation of mean diameter of zone of inhibition.

materials and control plates, with just one exception M + MoO_3. In the time interval of 36 hours, in most cases, there were significant differences; it is noteworthy that B + MoO_3, M + TiO_2 and M + MoO_3 were the most bioactive. In the period of 48 hours, in all cases, there were no significant differences between the materials and control plate, with just one exception M + TiO_2, highlighting that B + MoO_3, M + MoO_3, and M + TiO_2 were the most efficient biocides in inhibiting the proliferation of *S. aureus*.

Table 1 shows the results of the antibacterial and antifungal activity of materials against the tested pathogenic microorganisms; the results are exposed as the mean values obtained after 48 hours of assay.

The results from Table 1 show that the bioactivity of plant resins in pure state was effective and the addition of 10% w.t of oxides nanoparticles increased the efficiency of materials, as expected. Regarding the resin of *C. myrrha*, the antibiogram of bacteria and fungus under test corroborates the results obtained by Omer et al. [80] and in Alhussaini et al. [81]; concerning the resin of *B. papyrifera*, the results present in this study are in accordance with Camarda et al. [25], Abdallah et al. [82], Abdalah and Khalid [83], and de Rapper et al. [84]; and in relation to the resin of *S. benzoin* the results showed here are in accordance with the findings previously obtained by Dahni et al. [85] and De Rapper et al. [86].

3.2. SEM and EDXMA. Figure 2 shows the results of scanning electronic microscopy and energy-dispersive X-ray microanalysis.

According to Figure 2, the SEM analysis showed that part of oxides nanoparticles was encapsulated by the matrix of resins, and part remained heterogeneously dispersed over the surface of resins. Therefore, better ways of addition of oxides need to be studied, aiming for homogeneous nanostructure of the materials in the best way possible. One option is to increase the shearing forces during extrusion or premixing the content could improve the dispersant size and homogeneity in the dispersion by fractioning large agglomerates [87]. Another approach could be to feed the nanoparticles in suspension into the extrusion line [88]. During the printing of sample disks, an incomplete dispersion of the colloidal oxides in the disks was observed in the form of microsized domains of agglomerated nanoparticles; such agglomeration has previously been reported as a general problem for ceramic nanoparticles dispersed in polymers [89].

As exposed in Figure 3, the EDXMA analysis revealed information about the crystalline structure of samples.

According to Figure 3, the peaks identified at $2\theta = 15^\circ$ confirm the crystalline structure of the *B. papyrifera* [90]; the peaks found at $2\theta = 35^\circ$ and 45° confirm the molecular structure of *C. myrrha* [91]; the peaks at $2\theta = 35^\circ$ and 40° match with the chemical structure of *S. benzoin* [92]. No secondary phase was found samples, so it was possible to index the monoclinic phase of titanium oxide (PDF number 65-5714) and P25 anatase + rutile (PDF number 21-1272 and 21-1276, respectively). Those peaks at scattering angles of 25.26°, 36.94°, 48.05°, 53.89°, 55.06°, and 62.681° correspond to the reflections from the (101), (004), (200), (105), (211), and (204) crystalline planes of anatase (P25) and TiO_2 oxides [93]; it was possible to index the monoclinic phase of copper I (PDF number 89-5898) and molybdenum oxide (PDF number 13-345); the diffraction peak found at $2\theta = 26^\circ$ found in sample B + P25 is attributed to the hexagonal structure of graphite (002) [94]; the diffraction peaks found at $2\theta = 29{,}6^\circ$, $36{,}7^\circ$, and $42{,}5^\circ$ are attributed to Cu_2O crystalline planes (110), (200), and (220), respectively [95]. Lastly, the diffraction peaks at 2θ around 23.20°, 25.51°, 27.18°, 33.66°; 38.76°; 52.64°; 58.79°; and 67.28° correspond to (110), (040), (021), (111), (131), (211), (081), and (261); XRD standard data planes indexed to pure monocyclic and orthorhombic structure of MoO_3 [96].

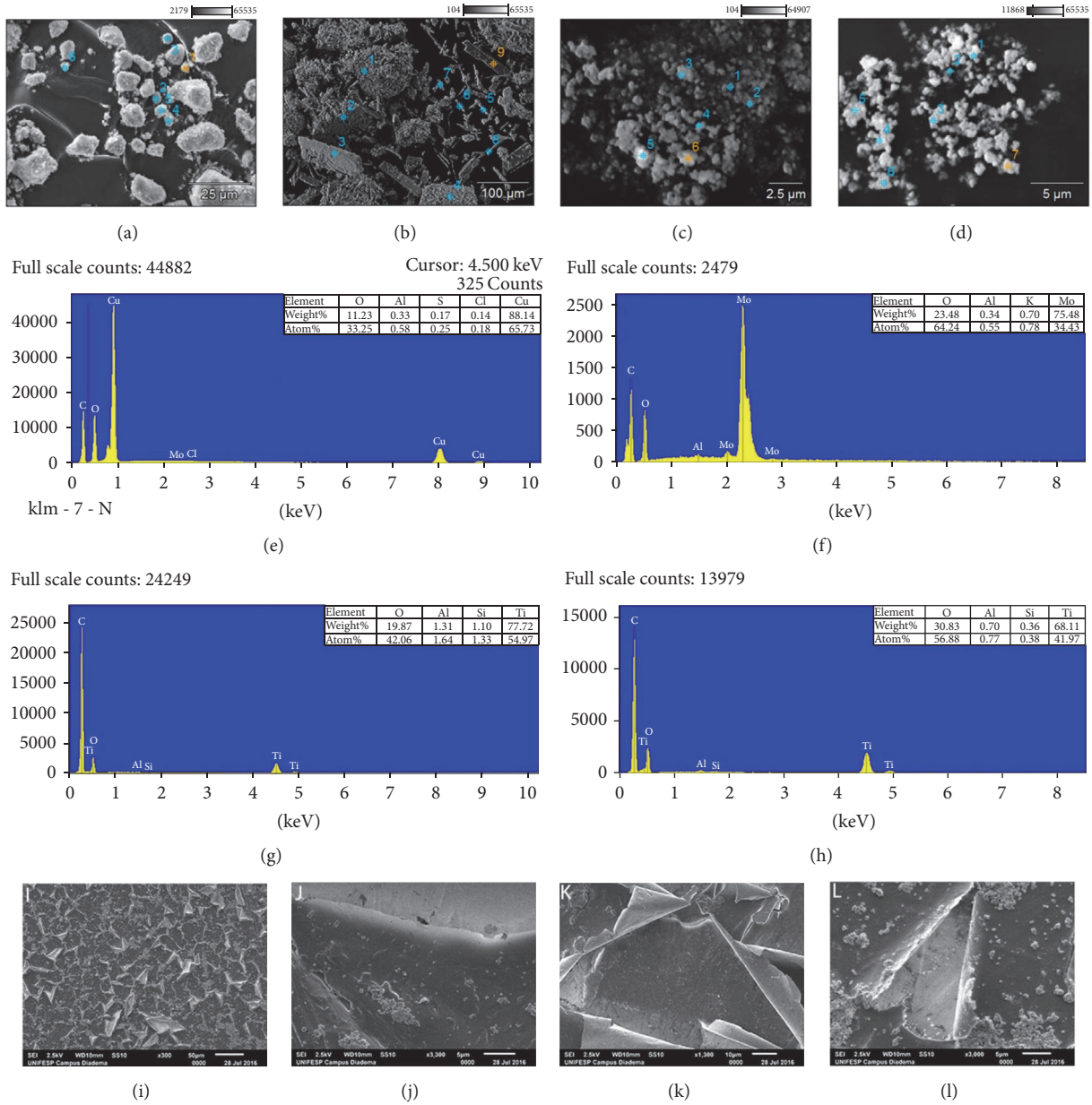

Figure 2: EDXMA analysis of metal oxides: Cu_2O (a); MoO_3 (b); P25 (c); TiO_2 (d); Cu_2O (e); MoO_3 (f); P25 (g); TiO_2 (h). SEM analysis of materials: B + P25 (i); M + TiO_2 (j); P + Cu_2O (k); B + MoO_3 (l).

3.3. UV-Vis and FTIR Spectroscopy. Figure 4 shows the UV-Visible spectrograms of samples.

According to Figure 4, the peaks at 350 nm to 420 nm confirm the molecular vibration of oleo-gum-resin of olibanum [97]; the peak found near of 390 nm with another prominent peak at 480 nm confirms the molecular vibration of myrrh extract [98]; the peak found at 350 nm with vibration extending to another peak at 450 nm confirms molecular vibration of benzoin resin [99]; the intensity of spectra obtained at wavelengths 350 nm is typical for the crystalline structure of anatase + rutile (P25) and titanium dioxide (TiO_2) [100]; the spectra showing intensity at wavelengths >300 nm typical for diametric and/or oligomeric species confirm the molecular vibration of MoO_3 [101]. Lastly, distinct peaks observed at 600 nm with stretching band until 800 nm confirm the vibration Cu_2O [102, 103].

Figure 5 shows FTIR spectrograms.

According to Figure 5, the FTIR spectrum of olibanum shows a peak at 3422.37 cm^{-1} indicating the presence of –OH– group, and the peak at 1705.33 cm^{-1} indicates the presence of carbonyl group The stretching band at 3428 cm^{-1} (O–H) and at 2930 cm^{-1} (C–H) and the bending bands of C–H appear at 1455 and 1378 cm^{-1} and the stretching band of C=O in carboxyl group appears at 1717 cm^{-1}, the stretching bands of C–O in carboxyl group are identified at 1243 cm^{-1}, and the stretching band of C=O at 1737 cm^{-1} indicates the presence of esters in olibanum resin [90].

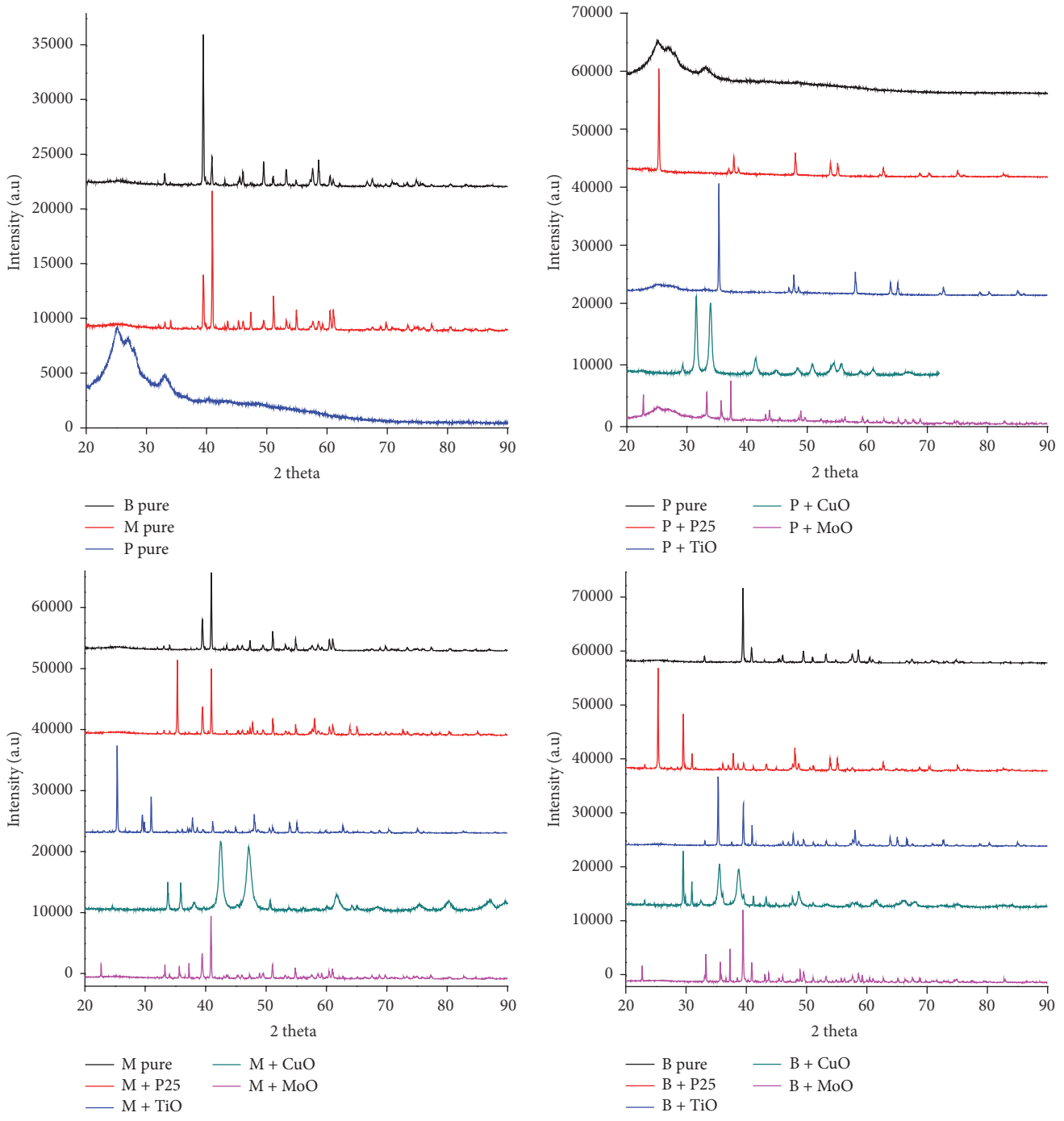

Figure 3: X-ray diffractograms of samples in pure state and also doped with metal oxides nanoparticles.

The FTIR spectrum of benzoin shows stretching band of carboxyl group (C=O) at 1719 cm^{-1}, and aromatic skeletal bands at 1601, 1516, and 1451 cm^{-1}, stretching band of C–O in carboxyl group at 1273 cm^{-1}, and a bending band at 712 cm^{-1} show a phenyl group (Ph–H) peaks identified at 1207 to 1441 cm^{-1} and 1376 to 1450 cm^{-1} confirming the presence of coniferyl benzoate [104]; the peak found near to 1650 cm^{-1} evidences an aliphatic unsaturation with strong C=C bonds, the peak near to 1610 cm^{-1} shows weak aromatic unsaturation [105], the peaks found at around 2872 and 2923 cm^{-1} can be attributed to C–H asymmetric and symmetric stretching vibration of methylene [106], also the band observed at around 1450 cm^{-1} is due to C–H stretching vibration of methylene bridge, a peak at 1560 cm^{-1} can be assigned to stretching vibration of a carboxylate group (–COOH) [107], the broad peaks at 3500 cm^{-1} 3.420 cm^{-1} can be assigned to

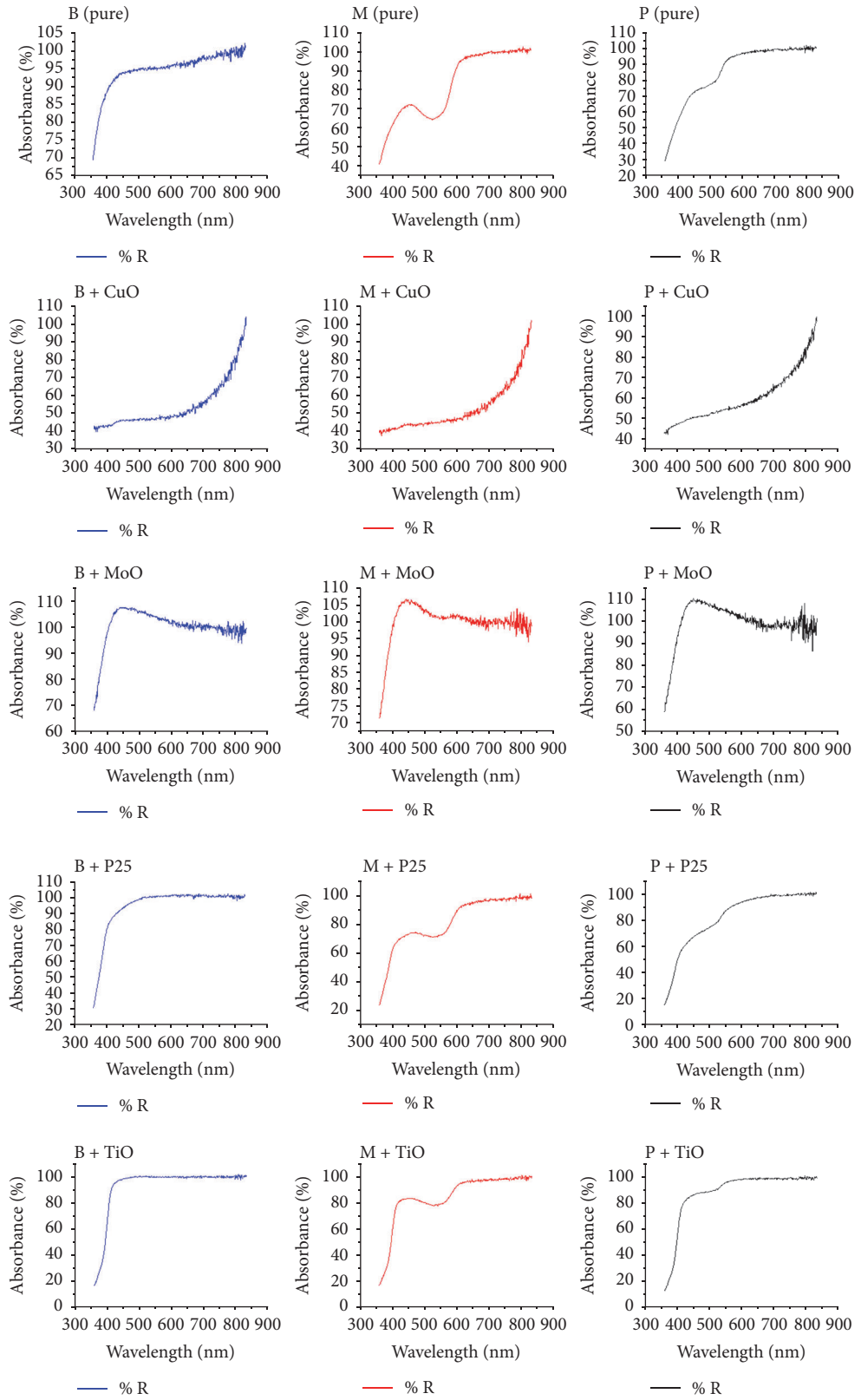

Figure 4: UV-Vis absorption spectra of samples in pure state and also doped with metal oxides nanoparticles.

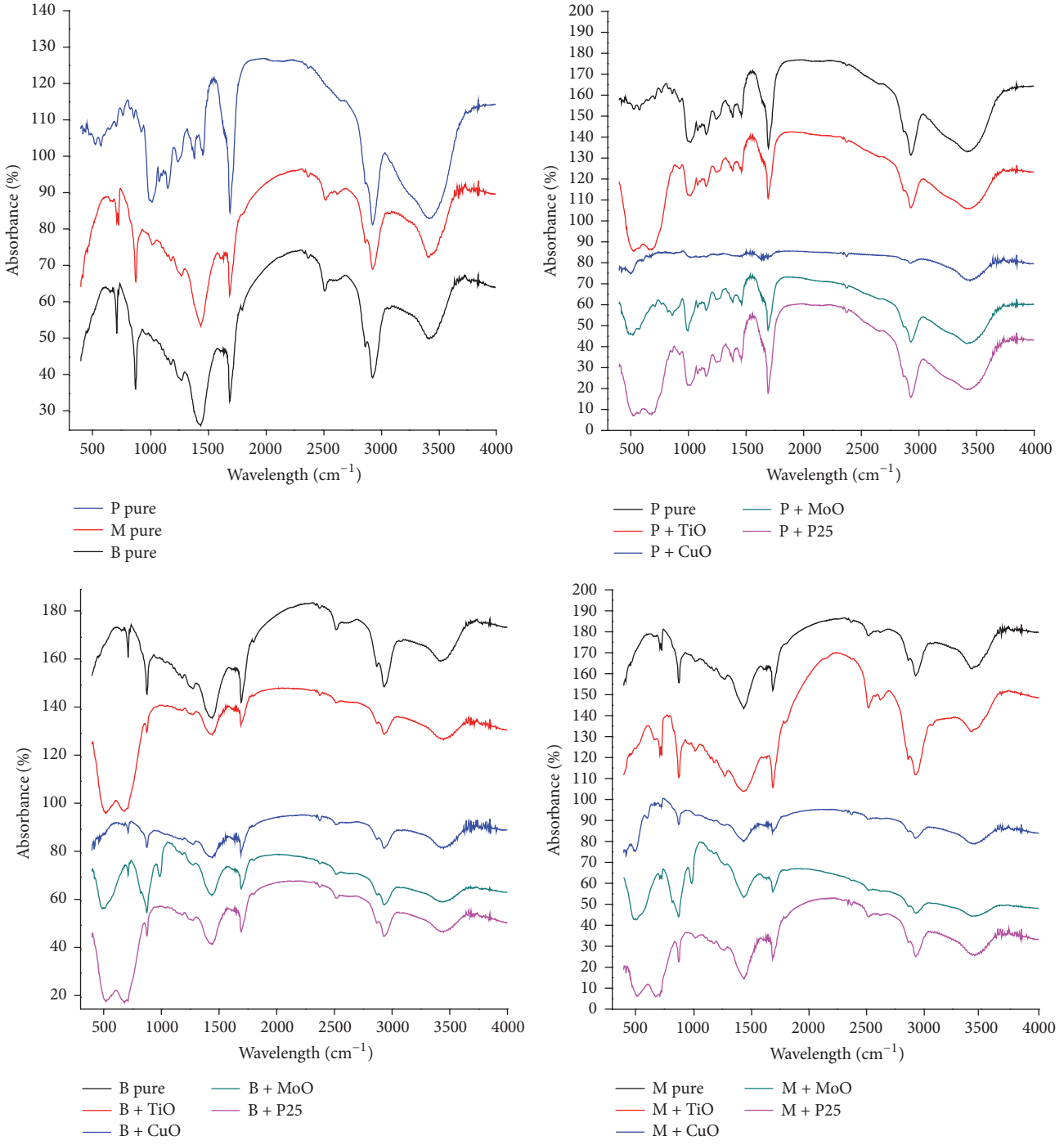

Figure 5: FTIR spectra of samples in pure state and also doped with metal oxides nanoparticles.

stretching of functional groups O–H [108], additionally peaks at 1580 to 1590 cm^{-1} correspond to stretching vibration of C=C–C aromatic rings [109], and lastly, a band observed at around 1400 cm^{-1} refers to C–H stretching vibration of vinyl [110] and broad peaks at 1070 cm^{-1} can be associated with stretching vibration of C–O–C [111].

The spectrum of myrrh shows the presence of broad bands located at 3.450, 1.630, and 1.550 cm^{-1} which are attributed to stretching of O–H, –COOH, and C=C and the shift of C=O vibration (symmetric stretching) of –COOH groups; an intense band at 1630 cm^{-1} confirms the molecular vibration of myrrh resin [105]; the stretching band identified at 1025 to 1200 cm^{-1} corresponds to the C–O stretching, while the weak bands at 1340 to 1450 cm^{-1} can be attributed to aliphatic hydrocarbons (CH_2 and CH_3) groups, groups of aldehydes (–CHO) and ketones (C=O), and the bending

modes of bonds in alcohols (O–H), phenols (–OH), and carboxylic acids (–COOH); the bands at 1620 and 1650 cm^{-1} correspond to aromatic rings, while the bands around 2920 to 2930 cm^{-1} are analogous to the asymmetric stretching of the C–H bonds [106]; the strong broad band appearing at 3440 cm^{-1} can be assigned to the stretching vibrations of various groups in alcohols (O–H) and phenols (–OH) [105, 112].

The FTIR spectra of resins doped with titanium oxide nanoparticles reveal a small peak at 1640 cm^{-1} and a large broad peak between 3450 and 3200 cm^{-1}, corresponding to the stretching vibrations of absorbed water, as well as hydroxyl (OH) groups present in the surface of TiO_2–P25 nanopowder [113]; the broad peak between 600 and 400 cm^{-1} can be assigned to the presence of Ti–O–Ti bonds [114]. Concerning the copper I oxide addition, the peaks found at 529 and 602 cm^{-1} denotes the (Cu–O) stretching vibration of monoclinic CuO phase; the broad peak at about 490–620 cm^{-1} (central at 548 cm^{-1}) was due to an overlap between Cu–O stretching vibration of Cu_2O/CuO and (–OH) hydroxyl vibrations at 490–510 cm^{-1} [115]; the peak found at 620 cm^{-1} is related to Cu_2O crystals [116], and the stretching bands found at 298 to 620 cm^{-1} match the crystalline structure of Cu_2O [117, 118].

Regarding molybdenum nanopowder, two peaks found at 876.5 and 595.8 cm^{-1} are assigned to MoO_3 phase [119]; the peak at 996 cm^{-1} was associated with the terminal stretching vibration of molybdenum in its oxidized form (MoO) that is an indication of layered MoO_3 phase; the bands at 867 cm^{-1} and 558 cm^{-1} are assigned to stretching vibrations and bending vibrations of the Mo–O–Mo units [120]; the bands at around 3435 cm^{-1} and 1614 cm^{-1} can be attributed to the stretching and bending vibrations of (O–H) hydroxyl groups in the adsorbed water [121].

It is important to emphasize that FTIR absorption bands of different compounds in wood resin exudates may be discriminated according to their responses to a given thermal stimulation, because different compounds usually respond in different ways to the same stimulation. For example, the spectral bands of a volatile compound will decrease synchronously if this compound evaporates when the sample is heated [122]; since plant samples usually are complex mixtures, signal-resolving methods are necessary to find the spectral features of compounds of interest in the signal-overlapped IR spectra.

3.4. Differential Scanning Calorimetry (DSC). Figure 6 shows the DSC curves of materials under analysis.

According to Figure 6, the thermophase diagram of myrrh in pure state presents characteristics of a semicrystalline polymer. The glass transition temperature (T_g) of this resin occurs at 75°C; from ambient temperature to this point, the material presents glassy behavior; it is hard, inflexible, and brittle, from 75°C to 300°C and this resin exhibits rubbery behavior, at this range; it is soft and flexible, from 300°C to 500°C, and the material presents viscoelastic state; the resin reaches its melting temperature (T_m) at 500°C. The peak at 150°C indicates a primary crystallization and the baseline change with a prominent peak at 300°C indicates a secondary crystallization, so the crystallization temperature (T_c) of this material occurs between 150°C and 300°C. In comparison to other available polymers, this resin shows similar characteristics to commercial polyurea.

The resin of benzoin also presents characteristics of a semicrystalline polymer such as polyurea. From ambient temperature till reaching 80°C (T_g), this biopolymers exhibits glassy state; from 80°C to 275°C, it presents rubbery state, with rigid crystalline phase and amorphous mobile phase; two exothermic peaks at 350°C and 420°C indicate that crystallizations occur at this temperature range (T_c), from 275°C to 500°C; the resin presents viscoelastic state; finally, this resin reaches its melting temperature (T_m) at 500°C.

Similarly, the resin of olibanum presents characteristics of semicrystalline polymers, such as polyester. Its glass transition temperature (T_g) occurs at 80°C; from this point forward until 300°C, this biopolymer presents rubbery state; two peaks at 300°C and 400°C indicate that crystallizations occur at this temperature range (T_c); lastly at 500°C, this biopolymer reaches its melting temperature (T_m).

When the temperature of resins reaches its T_m, the melting of crystallites occurs; at this point, the system power reaches the level needed to win the secondary intermolecular forces between the chains of the crystalline phase, destroying the regular packing structure, thereupon changing from rubbery state to viscous state. This transition only occurs in crystalline phase, so this interpretation only makes sense if it is applied to semicrystalline polymers [123].

It is evident that the addition of oxides nanoparticles will interfere in activation energy of particles by breaking existing chemical bonds between the atoms of each substance, thus favoring the occurrence of other chemical bonds and synthesis of a new substances, and also will influence the thermal-mechanical properties of samples (Ehrenstein et al., 2006) [124]. It will also depend on the degree of crystallinity, since higher crystallinity will result in a harder and more thermally stable but also more brittle material, whereas the amorphous regions provide certain elasticity and impact resistance [125, 126].

As exposed in the DSC signal, the addition of TiO_2 and P25 reveals peaks at 300°C and 500°C; at high temperatures, TiO_2 nanoparticles dehydrate and coarsen, the final stable phase upon grain growth being always rutile [127]. The overall process (phase transformation, water loss, and coarsening) is irreversible; the TiO_2 and P25 samples contain adsorbed water which has the properties of bulk liquid water and a small fraction bound very tightly, probably in the form of hydroxyl groups [128]. The addition of Cu_2O shows peaks at 300°C and 450°C, related to the removal of water from the surface [129] and the corrosion of copper nanoparticles [130], concerning the addition of MoO_3. The occurrence of peaks at 300°C and 500°C is due to the removal of water and recrystallizations of phases present in the nanopowder [131].

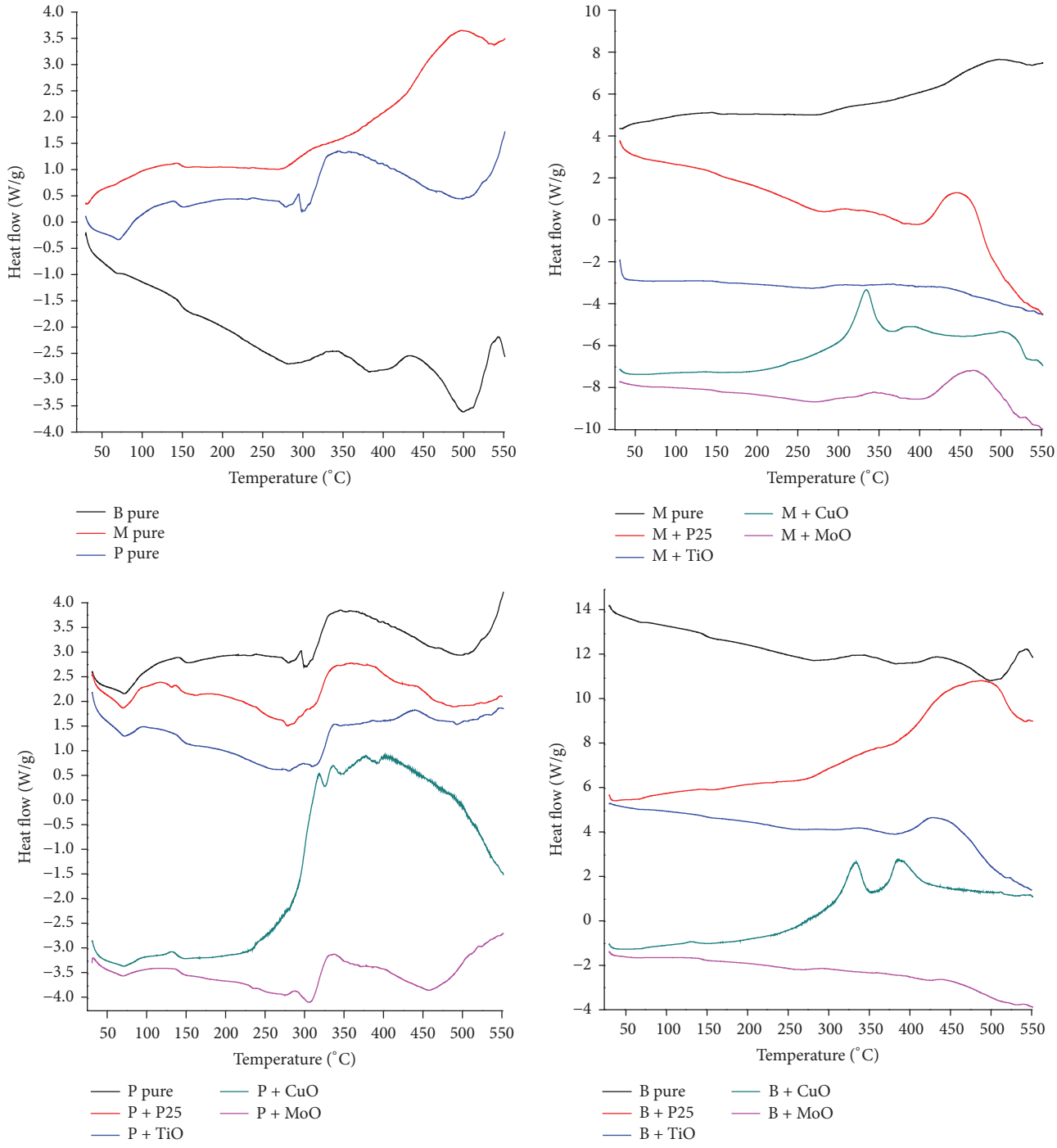

Figure 6: DSC phase diagram of samples in pure state and also doped with metal oxides nanoparticles.

In short, resins showed thermal behavior inherent to semicrystalline polymers such as polyester and polyurea; at some point, the molecules disposed in amorphous matrix obtain enough freedom of motion to spontaneously rearrange themselves into crystalline forms. This transition from amorphous solid to crystalline solid was evidenced by distinct exothermic peaks, as the temperature increases to 500°C samples, eventually reaching its melting point.

4. Conclusion

The biopolymers tested showed inherent characteristics of commercial available semicrystalline polymers; in most cases, the materials inhibited the proliferation of clinical pathogens under study, and, as expected, the addition of oxides nanoparticles increased the bacteriostatic effect. Although their addition was not well structured during the

production of filaments and disks, nanoparticles remained disorderly dispersed over the matrix of resins, in most cases being encapsulated by the same.

Conflicts of Interest

The authors declare that there are no conflicts of interest regarding the publication of this study.

Acknowledgments

The authors acknowledge the financial support from the Coordination of Improvement of Higher Level Personnel (CAPES, Brazil) through the Ph.D. scholarship granted.

References

[1] A. Muñoz-Bonilla and M. Fernández-García, "Polymeric materials with antimicrobial activity," *Progress in Polymer Science*, vol. 37, no. 2, pp. 281–339, 2012.

[2] O. Cuvas Apan, T. Z. Apan, and A. Apan, "In vitro antimicrobial activity of commonly used vasoactive drugs," *Journal of Clinical Anesthesia*, vol. 34, 2016.

[3] T.-W. Wan, Y. Tomita, N. Saita et al., "Emerging ST121/agr4 community-associated methicillin-resistant Staphylococcus aureus (MRSA) with strong adhesin and cytolytic activities: Trigger for MRSA pneumonia and fatal aspiration pneumonia in an influenza-infected elderly," *New Microbes and New Infections*, vol. 13, pp. 17–21, 2016.

[4] L. Gao, Y. Zhang, Y. Wang et al., "Reduction of PCN biosynthesis by NO in Pseudomonas aeruginosa," *Redox Biology*, vol. 8, pp. 252–258, 2016.

[5] E. Almaas, B. Kovács, T. Vicsek, Z. N. Oltvai, and A.-L. Barabási, "Global organization of metabolic fluxes in the bacterium *Escherichia coli*," *Nature*, vol. 427, no. 6977, pp. 839–843, 2004.

[6] A. M. Ibekwe, P. M. Watt, C. M. Grieve, V. K. Sharma, and S. R. Lyons, "Multiplex fluorogenic real-time PCR for detection and quantification of Escherichia coli O157:H7 in dairy wastewater wetlands," *Applied and Environmental Microbiology*, vol. 68, no. 10, pp. 4853–4862, 2002.

[7] X. Sun, C. Lei, L. Guo, and Y. Zhou, "Separable detecting of Escherichia coli O157H:H7 by a giant magneto-resistance-based bio-sensing system," *Sensors and Actuators, B: Chemical*, vol. 234, pp. 485–492, 2016.

[8] D. Williams and M. Lewis, "Pathogenesis and treatment of oral Candidosis," *Journal of Oral Microbiology*, vol. 3, no. 2011, article 5771, 2011.

[9] A. N. B. Ellepola, L. P. Samaranayake, and Z. U. Khan, "Extracellular phospholipase production of oral Candida albicans isolates from smokers, diabetics, asthmatics, denture wearers and healthy individuals following brief exposure to polyene, echinocandin and azole antimycotics," *Brazilian Journal of Microbiology*, vol. 47, no. 4, pp. 911–916, 2016.

[10] C. L. Ventola, "The antibiotic resistance crisis: part 2: management strategies and new agentsts," *Pharmacy and Therapeutics*, vol. 40, no. 5, pp. 344–352, 2015.

[11] T. D. Michl, K. E. S. Locock, S. S. Griesser, M. Haeussler, L. Meagher, and H. J. Griesser, "Bio-inspired antimicrobial polymers," in *Biosynthetic Polymers for Medical Applications*, pp. 87–127, Elsevier Science B.V, Amsterdam, Netherlands, 2016.

[12] D. Schillaci, V. Arizza, T. Dayton, L. Camarda, and V. Di Stefano, "In vitro anti-biofilm activity of Boswellia spp. oleogum resin essential oils," *Letters in Applied Microbiology*, vol. 47, no. 5, pp. 433–438, 2008.

[13] M. F. T. Medeiros and U. P. De Albuquerque, "The pharmacy of the Benedictine monks: The use of medicinal plants in Northeast Brazil during the nineteenth century (1823-1829)," *Journal of Ethnopharmacology*, vol. 139, no. 1, pp. 280–286, 2012.

[14] S. A. Sargin, E. Akçicek, and S. Selvi, "An ethnobotanical study of medicinal plants used by the local people of Alaşehir (Manisa) in Turkey," *Journal of Ethnopharmacology*, vol. 150, no. 3, pp. 860–874, 2013.

[15] Z. Hübsch, R. L. Van Zyl, I. E. Cock, and S. F. van Vuuren, "Interactive antimicrobial and toxicity profiles of conventional antimicrobials with Southern african medicinal plants," *South African Journal of Botany*, vol. 93, pp. 185–197, 2014.

[16] H. Kong, J. Yang, Y. Zhang, Y. Fang, K. Nishinari, and G. O. Phillips, "Synthesis and antioxidant properties of gum arabic-stabilized selenium nanoparticles," *International Journal of Biological Macromolecules*, vol. 65, pp. 155–162, 2014.

[17] A. A. Shahat, A. Y. Ibrahim, and M. S. Elsaid, "Polyphenolic content and antioxidant activity of some wild Saudi Arabian asteraceae plants," *Asian Pacific Journal of Tropical Medicine*, vol. 7, no. 7, pp. 545–551, 2014.

[18] A. N. Shikov, O. N. Pozharitskaya, V. G. Makarov, H. Wagner, R. Verpoorte, and M. Heinrich, "Medicinal Plants of the Russian Pharmacopoeia; Their history and applications," *Journal of Ethnopharmacology*, vol. 154, no. 3, pp. 481–536, 2014.

[19] S. Sultana, H. M. Asif, N. Akhtar, and K. Ahmad, "Medicinal plants with potential antipyretic activity: A review," *Asian Pacific Journal of Tropical Disease*, vol. 5, no. 1, pp. S202–S208, 2015.

[20] E. Özdemir and K. Alpınar, "An ethnobotanical survey of medicinal plants in western part of central Taurus Mountains: Aladaglar (Nigde-Turkey)," *Journal of Ethnopharmacology*, vol. 166, pp. 53–65, 2015.

[21] M. Bahmani, K. Saki, S. Shahsavari, M. Rafieian-Kopaei, R. Sepahvand, and A. Adineh, "Identification of medicinal plants effective in infectious diseases in Urmia, northwest of Iran," *Asian Pacific Journal of Tropical Biomedicine*, vol. 5, no. 10, pp. 858–864, 2015.

[22] P. Mendonça Pauletti, A. R. Araújo, M. C. M. Young, A. M. Giesbrecht, and V. Da Silva Bolzani, "nor-Lignans from the leaves of Styrax ferrugineus (Styracaceae) with antibacterial and antifungal activity," *Phytochemistry*, vol. 55, no. 6, pp. 597–601, 2000.

[23] M. A. Saeed and A. W. Sabir, "Antibacterial activities of some constituents from oleo-gum-resin of Commiphora mukul," *Fitoterapia*, vol. 75, no. 2, pp. 204–208, 2004.

[24] R. A. A. Mothana and U. Lindequist, "Antimicrobial activity of some medicinal plants of the island Soqotra," *Journal of Ethnopharmacology*, vol. 96, no. 1-2, pp. 177–181, 2005.

[25] L. Camarda, T. Dayton, V. Di Stefano, R. Pitonzo, and D. Schillaci, "Chemical composition and antimicrobial activity of some oleogum resin essential oils from Boswellia spp. (Burseraceae)," *Annali di Chimica*, vol. 97, no. 9, pp. 837–844, 2007.

[26] S. F. van Vuuren, G. P. P. Kamatou, and A. M. Viljoen, "Volatile composition and antimicrobial activity of twenty commercial frankincense essential oil samples," *South African Journal of Botany*, vol. 76, no. 4, pp. 686–691, 2010.

[27] M. P. Paraskeva, S. F. van Vuuren, R. L. van Zyl, H. Davids, and A. M. Viljoen, "The in vitro biological activity of selected South African Commiphora species," *Journal of Ethnopharmacology*, vol. 119, no. 3, pp. 673–679, 2008.

[28] J. Wanner, E. Schmidt, S. Bail et al., "Chemical composition and antibacterial activity of selected essential oils and some of their main compounds," *Natural Product Communications*, vol. 5, no. 9, pp. 1359–1364, 2010.

[29] T. Shen, G. Li, X. Wang, and H. Lou, "The genus Commiphora: a review of its traditional uses, phytochemistry and pharmacology," *Journal of Ethnopharmacology*, vol. 142, no. 2, pp. 319–330, 2012.

[30] S. Al-Daihan, M. Al-Faham, N. Al-shawi et al., "Antibacterial activity and phytochemical screening of some medicinal plants commonly used in Saudi Arabia against selected pathogenic microorganisms," *Journal of King Saud University - Science*, vol. 25, no. 2, pp. 115–120, 2013.

[31] A. A. Mohamed, S. I. Ali, F. K. EL-Baz, A. K. Hegazy, and M. A. Kord, "Chemical composition of essential oil and in vitro antioxidant and antimicrobial activities of crude extracts of Commiphora myrrha resin," *Industrial Crops and Products*, vol. 57, pp. 10–16, 2014.

[32] F. Wang, Y.-B. Wang, H. Chen, L. Chen, S.-W. Liang, and S.-M. Wang, "Two new triterpenoids from the resin of Styrax tonkinensis," *Journal of Asian Natural Products Research*, vol. 17, no. 8, pp. 823–827, 2015.

[33] L. O. Hanus, T. Rezanka, V. M. Dembitsky, and A. Moussaieff, "Myrrh -*Commiphora* chemistry," *Biomedical Papers*, vol. 149, no. 1, pp. 3–28, 2005.

[34] F. S. Li, D. L. Yan, R. R. Liu, K. P. Xu, and G. S. Tan, *Chemical Constituents of* Boswellia carterii *(Frankincense)*, vol. 8, pp. 25–27, 2007.

[35] D. Poeckel and O. Werz, "Boswellic acids: Biological actions and molecular targets," *Current Medicinal Chemistry*, vol. 13, no. 28, pp. 3359–3369, 2006.

[36] H. P. T. Ammon, "Boswellic acids in chronic inflammatory diseases," *Planta Medica*, vol. 72, no. 12, pp. 1100–1116, 2006.

[37] H. Safayhi and E.-R. Sailer, "Anti-inflammatory actions of pentacyclic triterpenes," *Planta Medica*, vol. 63, no. 6, pp. 487–493, 1997.

[38] K. H. C. Başer, B. Demirci, A. Dekebo, and E. Dagne, "Essential oils of some *Boswellia* spp., myrrh and opopanax," *Flavour and Fragrance Journal*, vol. 18, no. 2, pp. 153–156, 2003.

[39] G. Tayoub, I. Schwob, J.-M. Bessière et al., "Composition of volatile oils of Styrax (Styrax officinalis L.) leaves at different phenological stages," *Biochemical Systematics and Ecology*, vol. 34, no. 9, pp. 705–709, 2006.

[40] J.-J. Filippi, C. Castel, X. Fernandez, M. Rouillard, M. Gaysinski, and S. Lavoine-Hanneguelle, "An unusual acenaphthylene-type sesquiterpene hydrocarbon from Siam and Sumatra benzoin gum," *Phytochemistry Letters*, vol. 2, no. 4, pp. 216–219, 2009.

[41] D. L. Custódio and V. F. Veiga-Junior, "True and common balsams," *Brazilian Journal of Pharmacognosy*, vol. 22, no. 6, pp. 1372–1383, 2012.

[42] P. Burger, A. Casale, A. Kerdudo et al., "New insights in the chemical composition of benzoin balsams," *Food Chemistry*, vol. 210, pp. 613–622, 2016.

[43] S. Kumar and S. K. Gupta, "Rosin, A naturally derived excipient in drug delivery systems," *Polim. Med*, vol. 43, no. 1, pp. 45–48, 2013.

[44] S. K. Bajpai and M. Kumari, "A green approach to prepare silver nanoparticles loaded gum acacia/poly(acrylate) hydrogels," *International Journal of Biological Macromolecules*, vol. 80, pp. 177–188, 2015.

[45] C. Dong, X. Zhang, H. Cai, and C. Cao, "Facile and one-step synthesis of monodisperse silver nanoparticles using gum acacia in aqueous solution," *Journal of Molecular Liquids*, vol. 196, pp. 135–141, 2014.

[46] A. J. Kora and L. Rastogi, "Green synthesis of palladium nanoparticles using gum ghatti (Anogeissus latifolia) and its application as an antioxidant and catalyst," *Arabian Journal of Chemistry*, 2015.

[47] M. Bernela, M. Ahuja, and R. Thakur, "Enhancement of anti-inflammatory activity of glycyrrhizic acid by encapsulation in chitosan-katira gum nanoparticles," *European Journal of Pharmaceutics and Biopharmaceutics*, vol. 105, pp. 141–147, 2016.

[48] S. K. Bajpai, M. Jadaun, and S. Tiwari, "Synthesis, characterization and antimicrobial applications of zinc oxide nanoparticles loaded gum acacia/poly(SA) hydrogels," *Carbohydrate Polymers*, vol. 153, pp. 60–65, 2016.

[49] H. Joy Prabu and I. Johnson, "Plant-mediated biosynthesis and characterization of silver nanoparticles by leaf extracts of Tragia involucrata, Cymbopogon citronella, Solanum verbascifolium and Tylophora ovata," *Karbala International Journal of Modern Science*, vol. 1, no. 4, pp. 237–246, 2015.

[50] J. Rodríguez-Hernández, "Antimicrobial micro/nanostructured functional polymer surfaces," in *Nanobiomaterialsin Antimicrobial Therapy. Applications of Nanobiomaterials*, vol. 6, pp. 153–192, Elsevier Science B.V, Amsterdam, Netherlands, 2016.

[51] M. Quaresimin, R. Bertani, M. Zappalorto, A. Pontefisso, F. Simionato, and A. Bartolozzi, "Multifunctional polymer nanocomposites with enhanced mechanical and anti-microbial properties," *Composites Part B: Engineering*, vol. 80, article no. 3615, pp. 108–115, 2015.

[52] M. S. Ganewatta and C. Tang, "Controlling macromolecular structures towards effective antimicrobial polymers," *Polymer (United Kingdom)*, vol. 63, pp. A1–A29, 2015.

[53] D. F. Williams, "On the nature of biomaterials," *Biomaterials*, vol. 30, no. 30, pp. 5897–5909, 2009.

[54] R. K. Jha, P. K. Jha, K. Chaudhury, S. V. Rana, and S. K. Guha, "An emerging interface between life science and nanotechnology: present status and prospects of reproductive healthcare aided by nano-biotechnology," *Nano Reviews*, vol. 5, no. 1, article 22762, 2014.

[55] C. Buzea, I. I. Pacheco, and K. Robbie, "Nanomaterials and nanoparticles: sources and toxicity," *Biointerphases*, vol. 2, pp. MR17–MR71, 2007.

[56] L. Zhang, X. Wang, Y. Miao et al., "Magnetic ferroferric oxide nanoparticles induce vascular endothelial cell dysfunction and inflammation by disturbing autophagy," *Journal of Hazardous Materials*, vol. 304, pp. 186–195, 2016.

[57] J. J. Water, A. Bohr, J. Boetker et al., "Three-dimensional printing of drug-eluting implants: Preparation of an antimicrobial polylactide feedstock material," *Journal of Pharmaceutical Sciences*, vol. 104, no. 3, pp. 1099–1107, 2015.

[58] N. Sandler, I. Kassamakov, H. Ehlers, N. Genina, T. Ylitalo, and E. Haeggstrom, "Rapid interferometric imaging of printed drug laden multilayer structures," *Scientific Reports*, vol. 4, article no. 4020, 2014.

[59] T. M. Rankin, N. A. Giovinco, D. J. Cucher, G. Watts, B. Hurwitz, and D. G. Armstrong, "Three-dimensional printing surgical

instruments: are we there yet?" *Journal of Surgical Research*, vol. 189, no. 2, pp. 193–197, 2014.

[60] J. Yue, P. Zhao, J. Y. Gerasimov et al., "3D-Printable Antimicrobial Composite Resins," *Advanced Functional Materials*, vol. 25, no. 43, pp. 6756–6767, 2015.

[61] A. Ion, E. Andronescu, D. Řadulescu et al., "Biocompatible 3d matrix with antimicrobial properties," *Molecules*, vol. 21, no. 1, Article ID 21010115, 2016.

[62] M. Karl, D. Djuric, and K. Kolter, "Pharmaceutical Excipients for Hot-Melt Extrusion," *Pharmaceutical Technology*, vol. 35, no. 5, pp. 74–82, 2011.

[63] M. Wilson, M. A. Williams, D. S. Jones, and G. P. Andrews, "Hot-melt extrusion technology and pharmaceutical application," *Therapeutic Delivery*, vol. 3, no. 6, pp. 787–797, 2012.

[64] M. Lu, Z. Guo, Y. Li et al., "Application of hot melt extrusion for poorly water-soluble drugs: Limitations, advances and future prospects," *Current Pharmaceutical Design*, vol. 20, no. 3, pp. 369–387, 2014.

[65] M. Stanković, H. W. Frijlink, and W. L. J. Hinrichs, "Polymeric formulations for drug release prepared by hot melt extrusion: application and characterization," *Drug Discovery Today*, vol. 20, no. 7, article no. 1575, pp. 812–823, 2015.

[66] A. Melocchi, F. Parietti, A. Maroni, A. Foppoli, A. Gazzaniga, and L. Zema, "Hot-melt extruded filaments based on pharmaceutical grade polymers for 3D printing by fused deposition modeling," *International Journal of Pharmaceutics*, vol. 509, no. 1-2, pp. 255–263, 2016.

[67] J. Goole and K. Amighi, "3D printing in pharmaceutics: A new tool for designing customized drug delivery systems," *International Journal of Pharmaceutics*, vol. 499, no. 1-2, pp. 376–394, 2016.

[68] G. Mayer, "Rigid biological systems as models for synthetic composites," *Science*, vol. 310, no. 5751, pp. 1144–1147, 2005.

[69] E. Munch, M. E. Launey, D. H. Alsem, E. Saiz, A. P. Tomsia, and R. O. Ritchie, "Tough, bio-inspired hybrid materials," *Science*, vol. 322, no. 5907, pp. 1516–1520, 2008.

[70] J. Yuan and A. H. E. Müller, "One-dimensional organic-inorganic hybrid nanomaterials," *Polymer*, vol. 51, no. 18, pp. 4015–4036, 2010.

[71] C. Sanchez, B. Julián, P. Belleville, and M. Popall, "Applications of hybrid organic-inorganic nanocomposites," *Journal of Materials Chemistry*, vol. 15, no. 35-36, pp. 3559–3592, 2005.

[72] A. W. Bauer, W. M. Kirby, J. C. Sherris, and M. Turck, "Antibiotic susceptibility testing by a standardized single disk method," *The American Journal of Clinical Pathology*, vol. 45, no. 4, pp. 493–496, 1966.

[73] B. Bonev, J. Hooper, and J. Parisot, "Principles of assessing bacterial susceptibility to antibiotics using the agar diffusion method," *Journal of Antimicrobial Chemotherapy*, vol. 61, no. 6, pp. 1295–1301, 2008.

[74] J. Marotz, C. Lübbert, and W. Eisenbeiß, "Effective object recognition for automated counting of colonies in Petri dishes (automated colony counting)," *Computer Methods and Programs in Biomedicine*, vol. 66, no. 2-3, pp. 183–198, 2001.

[75] M. Putman, R. Burton, and M. H. Nahm, "Simplified method to automatically count bacterial colony forming unit," *Journal of Immunological Methods*, vol. 302, no. 1-2, pp. 99–102, 2005.

[76] S. Sieuwerts, F. A. M. De Bok, E. Mols, W. M. De Vos, and J. E. T. Van Hylckama Vlieg, "A simple and fast method for determining colony forming units," *Letters in Applied Microbiology*, vol. 47, no. 4, pp. 275–278, 2008.

[77] M. I. Rodrigues and A. F. Lemma, *Planejamento de experimentos e otimização de processos*, Cárita, Campinas, SP, Brazil, 2nd edition, 2009.

[78] C. A. Mucelin, *Estatística Elementar e experimental aplicada às tecnologias*, Medianeira, PR, Brazil, Valério, 2nd edition, 2006.

[79] M. G. Canteri, R. A. Althaus, J. S. Virgens Filho, E. A. Giglioti, and C. V. Godoy, "SASM - Agri: Sistema para anßlise e separaτπo de mΘdias em experimentos agrφcolas pelos mΘtodos ScoftKnott, Tukey e Duncan," *Revista Brasileira de Agrocomputaτπo*, vol. 1, no. 2, pp. 18–24, 2001.

[80] S. A. Omer, S. E. I. Adam, and O. B. Mohammed, "Antimicrobial activity of commiphora myrrha against some bacteria and candida albicans isolated from gazelles at king khalid wildlife research centre," *Research Journal of Medicinal Plant*, vol. 5, no. 1, pp. 65–71, 2011.

[81] M. S. Alhussaini, A. M. Saadabi, and M. I. Alghonaim, "An evaluation of the antimicrobial activity of commiphora myrrha nees (Engl.) oleo-gum resins from Saudi Arabia," *Journal of Medical Sciences (Faisalabad)*, vol. 15, no. 4, pp. 198–203, 2015.

[82] E. M. Abdallah, A. S. Khalid, and N. Ibrahim, "Antibacterial activity of oleo-gum resins of *Commiphora molmol* and *Boswellia papyrifera* against methicillin resistant *Staphylococcus aureus* (MRSA)," *AnnalidiChimica*, vol. 97, no. 9, pp. 837–844, 2009.

[83] E. M. Abdalah and A. E. Khalid, "A preliminary evaluation of the antibacterial effects of commiphora molmol and boswellia papyrifera oleo-gum resins vapor," *International Journal of Chemical and Biochemical Sciences*, vol. 1, pp. 1–15.

[84] S. de Rapper, S. F. Van Vuuren, G. P. P. Kamatou, A. M. Viljoen, and E. Dagne, "The additive and synergistic antimicrobial effects of select frankincense and myrrh oils—a combination from the pharaonic pharmacopoeia," *Letters in Applied Microbiology*, vol. 54, no. 4, pp. 352–358, 2012.

[85] R. Dahni, G. K. Eri, A. V. S. Gita Samira et al., "Anti-microbial screening of some novel benzoin derivatives," *International Journal of Advances in Pharmaceutical Research*, vol. 2, no. 12, pp. 639–642.

[86] S. De Rapper, G. Kamatou, A. Viljoen, and S. van Vuuren, "The *in vitro* antimicrobial activity of *Lavandula angustifolia* essential oil in combination with other aroma-therapeutic oils," *Evidence-based Complementary and Alternative Medicine*, vol. 2013, Article ID 852049, 10 pages, 2013.

[87] D. Shen, L. Fang, X. Chen, and Y. Tang, "Structure and properties of polyacrylic acid modified hydroxyapatite/liquid crystal polymer composite," *Journal of Reinforced Plastics and Composites*, vol. 30, no. 13, pp. 1155–1163, 2011.

[88] R. Baumgartner, A. Eitzlmayr, N. Matsko, C. Tetyczka, J. Khinast, and E. Roblegg, "Nano-extrusion: A promising tool for continuous manufacturing of solid nano-formulations," *International Journal of Pharmaceutics*, vol. 477, no. 1, pp. 1–11, 2014.

[89] T. Takayama, M. Todo, and A. Takano, "The effect of bimodal distribution on the mechanical properties of hydroxyapatite particle filled poly(L-lactide) composites," *Journal of the Mechanical Behavior of Biomedical Materials*, vol. 2, no. 1, pp. 105–112, 2009.

[90] S. Mohanty and M. G. Krishna, "Proximate analysis and standardization of plant exudates: gum olibanum and gum dikamali," *International Journal of Pharmaceutical Sciences Review and Research*, vol. 24, no. 1, pp. 172–176, 2014.

[91] A. M. Atta, H. A. Al-Lohedan, and S. A. Al-Hussain, "Synthesis of stabilized myrrh-capped hydrocolloidal magnetite nanoparticles," *Molecules*, vol. 19, no. 8, pp. 11263–11278, 2014.

[92] J. Du, H. Singh, and T.-H. Yi, "Antibacterial, anti-biofilm and anticancer potentials of green synthesized silver nanoparticles using benzoin gum (Styrax benzoin) extract," *Bioprocess and Biosystems Engineering*, vol. 39, no. 12, pp. 1923–1931, 2016.

[93] Z. He, W. Que, J. Chen, Y. He, and G. Wang, "Surface chemical analysis on the carbon-doped mesoporous TiO2 photocatalysts after post-thermal treatment: XPS and FTIR characterization," *Journal of Physics and Chemistry of Solids*, vol. 74, no. 7, pp. 924–928, 2013.

[94] J. Hu, Y. Bandog, J. Zhan, C. Zhi, and D. Golberg, "Carbon nanotubes as nanoreactors for fabrication of single-crystalline Mg3N2 nanowires," *Nano Letters*, vol. 6, no. 6, pp. 1136–1140, 2006.

[95] D. Cao, N. Nasori, Z. Wang et al., "Facile surface treatment on Cu2O photocathodes for enhancing the photoelectrochemical response," *Applied Catalysis B: Environmental*, vol. 198, pp. 398–403, 2016.

[96] M. Balaji, J. Chandrasekaran, and M. Raja, "Role of substrate temperature on MoO3 thin films by the JNS pyrolysis technique for P-N junction diode application," *Materials Science in Semiconductor Processing*, vol. 43, pp. 104–113, 2016.

[97] A. J. Kora, R. B. Sashidhar, and J. Arunachalam, "Aqueous extract of gum olibanum (*Boswellia serrata*): a reductant and stabilizer for the biosynthesis of antibacterial silver nanoparticles," *Process Biochemistry*, vol. 47, no. 10, pp. 1516–1520, 2012.

[98] I. M. El-Sherbiny, E. Salih, and F. M. Reicha, "Green synthesis of densely dispersed and stable silver nanoparticles using myrrh extract and evaluation of their antibacterial activity," *Journal of Nanostructure in Chemistry*, vol. 3, no. 8, pp. 1–7, 2013.

[99] M. Hovaneissian, P. Archier, C. Mathe, G. Culioli, and C. Vieillescazes, "Analytical investigation of styrax and benzoin balsams by HPLC-PAD-fluorimetry and GC-MS," *Phytochemical Analysis*, vol. 19, no. 4, pp. 301–310, 2008.

[100] Y. Man, L. Mu, Y. Wang, S. Lin, G. L. Rempel, and Q. Pan, "Synthesis and characterization of rutile titanium dioxide/polyacrylate nanocomposites for applications in ultraviolet light-shielding materials," *Polymer Composites*, vol. 36, no. 1, pp. 8–16, 2015.

[101] J. P. Thielemann, T. Ressler, A. Walter, G. Tzolova-Müller, and C. Hess, "Structure of molybdenum oxide supported on silica SBA-15 studied by Raman, UV-Vis and X-ray absorption spectroscopy," *Applied Catalysis A: General*, vol. 399, no. 1-2, pp. 28–34, 2011.

[102] M. S. M. Suan, M. R. Johan, N. L. Hawari, and H. A. Ching, "Annealing effects on the properties of copper oxide thin films prepared by chemical deposition," *International Journal of Electrochemical Science*, vol. 6, no. 12, pp. 6094–6104, 2011.

[103] G. Varuguese, V. Rini, S. P. Suraj, and K. T. Usha, "Characterization and optical studies of copper oxide nanostructures doped with lanthanum ions," *Advances in Materials Science*, vol. 14, no. 4, pp. 49–60, 2014.

[104] J.-B. Chen, Q. Zhou, and S.-Q. Sun, "Direct chemical characterization of natural wood resins by temperature-resolved and space-resolved Fourier transform infrared spectroscopy," *Journal of Molecular Structure*, vol. 1115, pp. 55–62, 2016.

[105] H. G. M. Edwards and M. J. Falk, *Spectrochimica Acta-Part A: Molecular and Biomolecular Spectroscopy*, vol. 53, Elsevier, Amsterdam, Netherlands, 1997.

[106] M. Xue, X. Zhang, Z.-F. Wu, H. Wang, X. Ding, and X.-Y. Tian, "Preparation and flame retardancy of polyurethane/POSS nanocomposites," *Chinese Journal of Chemical Physics*, vol. 26, no. 4, pp. 445–450, 2013.

[107] F. Jiang, X. Wang, and D. Wu, "Design and synthesis of magnetic microcapsules based on n-eicosane core and Fe3O4/SiO2 hybrid shell for dual-functional phase change materials," *Applied Energy*, vol. 134, pp. 456–468, 2014.

[108] S. N. Kharat and V. D. Mendhulkar, ""synthesis, characterization and studies on antioxidant activity of silver nanoparticles using Elephantopus scaber leaf extract"," *Materials Science and Engineering C*, vol. 62, pp. 719–724, 2016.

[109] C. M. Baicea, V. I. Luntraru, D. I. Vaireanu, E. Vasile, and R. Trusca, "Composite membranes with poly(ether ether ketone) as support and polyaniline like structure, with potential applications in fuel cells," *Central European Journal of Chemistry*, vol. 11, no. 3, pp. 438–445, 2013.

[110] B. Guan, P. A. Latif, and T. Yap, "Physical preparation of activated carbon from sugarcane bagasse and corn husk and its physical and chemical characteristics," *Int. J. Eng. Res. Sci. Technol*, vol. 2, pp. 1–14, 2013.

[111] H. Yang, R. Yan, H. Chen, D. H. Lee, and C. Zheng, "Characteristics of hemicellulose, cellulose and lignin pyrolysis," *Fuel*, vol. 86, no. 12-13, pp. 1781–1788, 2007.

[112] M. Yilmaz, H. Turkdemir, M. A. Kilic et al., "Biosynthesis of silver nanoparticles using leaves of Stevia rebaudiana," *Materials Chemistry and Physics*, vol. 130, no. 3, pp. 1195–1202, 2011.

[113] Q. Chen and N. L. Yakovlev, "Adsorption and interaction of organosilanes on TiO2 nanoparticles," *Applied Surface Science*, vol. 257, no. 5, pp. 1395–1400, 2010.

[114] F. Cheng, S. M. Sajedin, S. M. Kelly, A. F. Lee, and A. Kornherr, "UV-stable paper coated with APTES-modified P25 TiO2 nanoparticles," *Carbohydrate Polymers*, vol. 114, pp. 246–252, 2014.

[115] A. Pendashteh, M. F. Mousavi, and M. S. Rahmanifar, "Fabrication of anchored copper oxide nanoparticles on graphene oxide nanosheets via an electrostatic coprecipitation and its application as supercapacitor," *Electrochimica Acta*, vol. 88, pp. 347–357, 2013.

[116] J.-J. Ruan, Y.-Q. Huo, and B. Hu, "Three-dimensional Ni(OH)2/Cu2O/CuO porous cluster grown on nickel foam for high performance supercapacitor," *Electrochimica Acta*, vol. 215, pp. 108–113, 2016.

[117] T. Yu, X. Zhao, Z. X. Shen, Y. H. Wu, and W. H. Su, "Investigation of individual CuO nanorods by polarized micro-Raman scattering," *Journal of Crystal Growth*, vol. 268, no. 3-4, pp. 590–595, 2004.

[118] M. A. Dar, S. H. Nam, Y. S. Kim, and W. B. Kim, "Synthesis, characterization, and electrochemical properties of self-assembled leaf-like CuO nanostructures," *Journal of Solid State Electrochemistry*, vol. 14, no. 9, pp. 1719–1726, 2010.

[119] Y. Zhu, X. Li, D. Zhang et al., "Tuning the surface charges of MoO3 by adsorption of polyethylenimine to realize the electrophoretic deposition of high-exothermic Al/MoO3 nanoenergetic films," *Materials and Design*, vol. 109, pp. 652–658, 2016.

[120] C. V. Subba Reddy, E. H. Walker Jr., C. Wen, and S.-I. Mho, "Hydrothermal synthesis of MoO3 nanobelts utilizing poly(ethylene glycol)," *Journal of Power Sources*, vol. 183, no. 1, pp. 330–333, 2008.

[121] L. Wang, X. Zhang, Y. Ma, M. Yang, and Y. Qi, "Rapid microwave-assisted hydrothermal synthesis of one-dimensional MoO3 nanobelts," *Materials Letters*, vol. 164, pp. 623–626, 2016.

[122] J.-B. Chen, S.-Q. Sun, and Q. Zhou, "Data-driven signal-resolving approaches of infrared spectra to explore the macroscopic and microscopic spatial distribution of organic and inorganic compounds in plant," *Analytical and bioanalytical chemistry*, vol. 407, no. 19, pp. 5695–5706, 2015.

[123] S. V. Canevarolo Junior, *Polimer Science*, Artliber, São Paulo, SP, Brazil, 2nd edition, 2006.

[124] G. W. Ehrenstein, *Polymericmaterials:Structure, Properties, Applications*, Hanser Gardner Publications, Cincinnat, Ohio, USA, 2001.

[125] G. Menges, E. Haberstroh, W. Michaeli, and E. Schmachtenberg, *Plastics Materials Science*, Carl Hanser Verlag, Munchen, Germany.

[126] C. E. Carraher and R. B. Seymour, *Eymour/Carraher'Spolymerchemistry*, Marcel Dekke, New York, NY, USA, 6th edition, 2003.

[127] C. Marinescu, A. Sofronia, C. Rusti et al., "DSC investigation of nanocrystalline TiO2 powder," *Journal of Thermal Analysis and Calorimetry*, vol. 103, no. 1, pp. 49–57, 2011.

[128] G. Madras, B. J. McCoy, and A. Navrotsky, "Kinetic model for TiO2 polymorphic transformation from anatase to rutile," *Journal of the American Ceramic Society*, vol. 90, no. 1, pp. 250–255, 2007.

[129] N. Topnani, S. Kushwaha, and T. Athar, "Wet synthesis of copper oxide nanopowder," *International Journal of Green Nanotechnology: Materials Science and Engineering*, vol. 1, no. 2, pp. M67–M73, 2009.

[130] Y. Wan, X. Wang, H. Sun, Y. Li, K. Zhang, and Y. Wu, "Corrosion behavior of copper at elevated temperature," *International Journal of Electrochemical Science*, vol. 7, no. 9, pp. 7902–7914, 2012.

[131] A. Lagashetty, V. Havanoor, S. Basavaraja, and A. Venkataraman, "Synthesis of MoO3 and its polyvinyl alcohol nanostructured film," *Bulletin of Materials Science*, vol. 28, no. 5, pp. 477–481, 2005.